

Chapter 10

Disorder in Smectite, Illite/Smectite, and Illite

If you have read this far, you know that the overwhelming emphasis in this book is on the interpretation of basal or $00l$ diffraction patterns from oriented clay mineral aggregates. This approach is justified because these patterns are the most diagnostic for both the simple and the mixed-layered clay minerals. Basal reflections from well-oriented samples are strong, producing excellent diffractograms with little effort on the part of the experimentalist. The peaks are strong because many crystallites are oriented so that they contribute to a given $00l$ reflection. Three-dimensional studies, on the other hand, require randomly oriented aggregates, and all the peaks are weak because only a small fraction of the crystallites have the required orientation for any given reflection.

Interferences from nonclay minerals are more severe in diffractograms from randomly oriented aggregates. Consider a mixture of quartz and a clay mineral. The quartz is randomly oriented in both oriented and randomly oriented preparations, so peak intensities are the same for both. But a clay mineral gives very strong reflections from the oriented aggregate, producing a high peak intensity ratio of clay mineral to quartz. In random orientation, peak intensities are “correct” for both, weakening the clay mineral relative to quartz reflections. Another problem is that the similarities of atomic structures in the X - Y plane of many of the clay minerals cause severe peak interferences among the clay minerals in a mixture.

Three-dimensional studies are difficult and not routine at present. You would not log a core with them. And you will have to give up on many samples; they simply present too many interference problems to be amenable to study. What kinds of rocks can be dealt with? The easiest are the bentonites and K-bentonites because the clay-sized fractions are almost monomineralic. Clay minerals from sandstones can often be extracted by gentle disaggregation procedures to yield suitable materials. The clay-sized fractions from carbonate rocks are often relatively free from detrital components, and some contain simple clay mineralogies. Unfortunately, the most important sedimentary rocks, shales, usually have such complex mixtures of detrital and diagenetic minerals in their fine-grain sizes that many of them are so difficult to deal with by any XRD methods (but see Grathoff and Moore, 1996) that high-resolution transmission electron microscopy has been the method for

their study.

The previous paragraphs make it clear why so little is known about the geological significance of disorder in illite and illite/smectite (I/S). It is true that we recognize a *IMd* variety of illite, but the term *IMd* is often used as a qualitative label for what is in fact a member of a continuous series. However, the various types and amounts of disorder can be identified and quantified by means of calculated three-dimensional diffraction patterns. This is analogous to the way that NEWMOD[©] has been used to unravel the one-dimensional character of mixed-layered clay minerals. In this chapter, you will see the results produced by a computer program called WILDFIRE[©] (Reynolds, 1993, 1994), which is the three-dimensional analog of NEWMOD[©] (Reynolds, 1985). For those of you who wish to pursue the subject of disorder in lamellar crystals and its mathematical development, the text by Drits and Tchoubar (1990) is state of the art on this subject.

We recognize four types of disorder in smectite, illite, and I/S. The first is mixed-layering of illite with smectite, and that has been discussed in earlier chapters. The other three are (1) turbostratic stacking in smectite and illite/smectite; (2) rotational disorder in illite, which leads in the limit to the *IMd* species; and (3) interstratification of two different kinds of illite layers. The last category means that much of the illite/smectite that we have been identifying for years is really mixed-layered illite₁/illite₂/smectite. Now that you have finally reached the point at which you understand illite/smectite, it seems unfair to tell you that the designation illite/smectite is really an oversimplification, but we think it is.

SMALL CRYSTALS IN RECIPROCAL SPACE

The diffraction model that follows for disordered structures in reciprocal space superficially looks like the traditional Ewald construction, but it is not (recall discussion of reciprocal space in Chapter 3, p. 80). It has been modified to eliminate the Ewald sphere and its relation to the diffraction angle, 2θ . In addition, the planar indices h , k , and l are treated as continuous variables; *i.e.*, they are not limited to integral values. This is the construction formulated by Méring and Brindley (1951). It deals with a randomly oriented multicrystallite *powder* in reciprocal space in such a way that intensity can be summed over all values of h , k , and l that produce the same diffraction angle.

First, let's consider diffraction in three dimensions. A simple formulation that can be transformed to deal with disorder but will not be here (see Reynolds, 1993, for that development), is as follows:

$$I(hkl) = |F(hkl)|^2 \frac{\sin^2(\pi N_1 h)}{\sin^2(\pi h)} \frac{\sin^2(\pi N_2 k)}{\sin^2(\pi k)} \frac{\sin^2(\pi N_3 l)}{\sin^2(\pi l)} \quad (10.1)$$

We neglect the Lorentz-polarization factor. The three N terms refer to the dimensions of a crystal expressed by the numbers of unit cells in the X , Y , and Z directions. The sine-squared quotients make up the three-dimensional interference function. The reciprocal intercepts of the diffracting plane, h , k , and l , can have any value. Thus we can deal with diffraction from a plane with intercepts [e.g., 1.05, 2.13, 4.88, which, of course, is not the (125) plane—but close]. Such nonintegral intercepts make no sense for thick crystals because they describe a plane that would produce no measurable diffraction (recall the discussion associated with Fig. 3.13, p. 85). But as the crystals become smaller, the peaks become broader, and that means that diffraction occurs when the (125) is not quite lined up, or, in other words, when the diffracting plane is not strictly the (125) but one of a continuous series of planes whose orientations are clustered about the (125), each of which makes its intensity contribution with an incremental change in the diffraction angle. The farther the diffraction angle is from the precise value for the (125), the weaker the intensity becomes due to the effect of the interference function. If the crystal size is so small that crystallites consist of only one unit cell, there is no Bragg diffraction and scattering will be recorded from any orientation of the crystal. In this case h , k , and l serve to locate a plane whose only requirement for producing recordable scattering is that it has the same angle of incidence, with respect to the primary beam, as its angle with respect to the “diffracted” beam.

The structure factor F is given by Eq. (10.2), which is the three-dimensional form of F for a centrosymmetric structure (recall discussion of the one-dimensional structure factor from Chapter 3, p. 91). The sum is taken over all atoms (j), where f is the temperature-corrected scattering factor for each and the quantities x , y , and z are the three-dimensional atomic coordinates expressed in Å.

$$F(hkl) = \sum_j f_j \cos \left\{ 2\pi \left(h x_j / a + k y_j / b + l z_j / c \right) \right\} \quad (10.2)$$

Let us return to Eq. (10.1). For very large crystals, each of the sine-squared quotients has the constant value of N^2 , if h , k , and l are integers, and if all the peaks have the same breadths (excluding instrumental effects). A set of $F(hkl)$ values is all that is needed to characterize the diffraction characteristics of the crystal, and that is what is measured for a single crystal structure determination. But if the crystal is small, the sine-squared quotients have finite values when h , k , and l are nonintegral; intensity falls off to zero when $h = h_0 \pm 1/N_1$; $k = k_0 \pm 1/N_2$; and $l = l_0 \pm 1/N_3$ (zero subscripts denote the integral values of h , k , and l). Two questions for you: (1) What are the plus-or-minus limits for h , k , and l if the crystals are infinitely large ($N = \infty$)? and (2) Why should diffraction peak breadths be inversely proportional to crystallite dimensions as given by the Scherrer equation on p. 87?

One-dimensional intensity calculations are simple because for any value of l there is only one value of 2θ . Consequently, we calculate intensity over a range of l and convert these l values to 2θ equivalents by means of the Bragg law $l\lambda = 2d\sin\theta$, or $\sin(\theta) = l\lambda/2d$, or $2\theta = 2\sin^{-1}(l\lambda/2d)$. But how to deal with 2θ in Eq. (10.1)? There are an infinite number of h , k , and l nonintegral values that produce the same 2θ (or the same d). A summation is required over all values of h , k , and l that produce a given d or 2θ . Because computers cannot handle infinite numbers of calculations some cleverness is required in the algorithm. We cannot go into this here, but see Reynolds (1993) if you want the details of how this can be done.

An orthorhombic (no nonorthogonal axes) structure in two dimensions serves as a simplified example of such a summation. Figure 10.1 shows the two orthogonal reciprocal space dimensions Z^* and X^* . Visualize the axis Y^* as normal to the plane of the figure, and set the two-dimensional $X^* - Z^*$ plane at $k = 0$. Remember that the increments labeled h and l are $1/d(100)$ and $1/d(001)$, respectively. This arrangement deals with reflections of the type $h0l$. Reciprocal lattice spots are shown as ellipses, not as the points that a large crystal would produce. The shape of the spots is the reciprocal of the crystal shape (what else would you expect in reciprocal space?), and for this example, the crystal is thicker in the X direction than it is in the Z direction. The spots show diagrammatically that the intensities are stronger near their centers. The structure factor, F , is not included in this construction, so the spots represent only the three-dimensional interference function part of Eq. (10.1). Including F would have made the spots differ from each other in absolute intensity (and some might be missing due to extinctions that are characteristic of the symmetry of the unit cell). We remind you again that this construction represents reciprocal space, so the length of the two vectors shown with their origins at 0,0 is equal to $1/d$ or d^* . For $c = 10 \text{ \AA}$ and $a = 6 \text{ \AA}$, the length of these vectors in normal space is 2.92 \AA , corresponding to $2\theta = 30.65^\circ$, $\text{CuK}\alpha$. (Use a ruler and see if you can figure this out.)

We will calculate the intensity of diffraction from a randomly oriented powder of small crystals at one specific diffraction angle, 30.65° as in Fig. 10.1. A randomly oriented powder means that there are crystals suitably oriented to produce any reflection of the type $k0l$ at the proper 2θ ; and because the crystals are small (the spots are large), the measured intensity will include diffraction from some spots that are just nicked by the intensity summation vector. Or, to put it another way, the summation of the intensity at 30.65° will catch just the edges of some of the broad Bragg reflections.

Equation (10.1) must be summed for all values of h and l that lie on the circular arc whose radius is given by the magnitude of the vector d^* or $1/d = 0.343$. Visualize the vector as rotating through the angles 0° to 90° , where 0° is defined as coincidence with Z^* . For each angular increment, we compute h and l , substitute those into Eq. (10.1), and add the resulting intensity to the accumulating sum. Our intensity includes the integrated 103 reflection

because the arc passes right through it. In addition, the arc cuts through a significant portion of the 201 maximum adding again to the sum. And finally, the integration just catches the “outside” edge of the 200 diffraction region.

We have computed the intensity at $30.65^\circ 2\theta$, but we need to go on and build up an entire diffraction pattern. The summation is set to zero, the vector d^* is increased by a small amount corresponding to an increased 2θ , and the summation is repeated, giving the intensity at the next 2θ value.

The calculations are more complicated for three dimensions. The vector must be rotated about the axis Z^* for each angular change in the X^*-Z^* plane. Each rotation generates a circle of summation lying in the plane normal to Z^* . The radii, *i.e.*, d^* , of the successive circles increase as the tip of the vector is moved clockwise from Z^* to X^* (Fig. 10.2). The summation of intensity for a specific 2θ includes the sums of all portions of the spots that lie on a spherical surface whose radius is d^* . Figure 10.2 shows the construction. It illustrates the commonly used nomenclature that designates the columns of reciprocal lattice spots along Z^* as “rods.” Note: a common misunderstanding is that the spherical surface shown on Fig. 10.2 is the sphere of reflection or the Ewald sphere. It is not. It is a surface such that all points on it represent hkl coordinates that have identical values of d .

The constructions of Figs. 10.1 and 10.2 are worth exploring. Suppose that a calculated $00l$ or basal diffraction pattern is required. Then the orientation of the vector is fixed coincident with Z^* and is increased in length

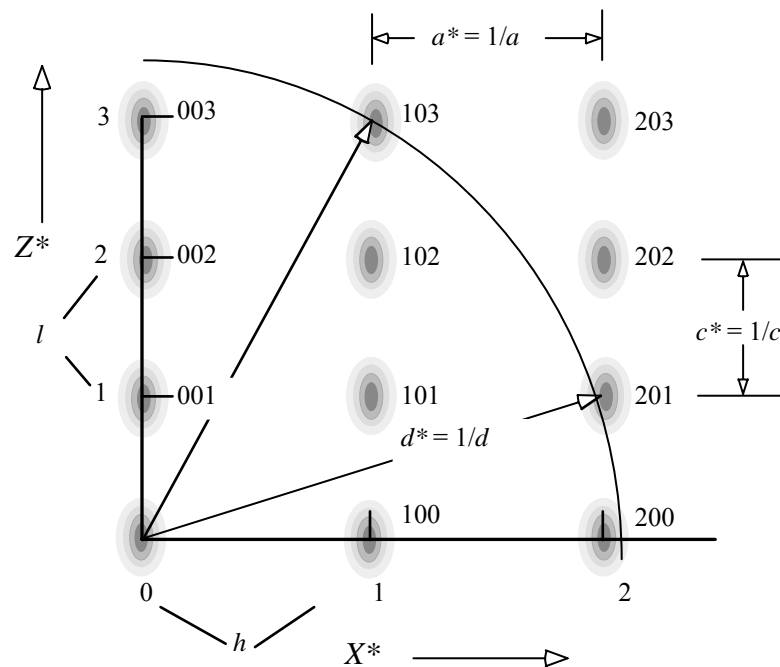


Fig. 10.1. Reciprocal lattice representation of a crystal of finite size and the summation vector for calculating the intensity of diffraction from a randomly oriented powder.

incrementally for a calculation of the intensity at each 2θ . How would a

powder of very large crystals appear? The spots would be exceedingly small dots, and the only intensity recorded at 30.65° would be from the 103 reflection—and perhaps even that would be missed and show up at a different vector length corresponding to, say, 30.60° . What if the crystals were smaller in both the X and Z directions? Well, it depends on how much smaller, but perhaps the calculated intensity would then contain additional components from the 003 and 202 reflections. What if all the crystals were so small that they consisted of separate unit cells ($N=1$)? There would be no spots. They would merge into a uniform field of non-Bragg scattering, and the diffraction pattern would then consist of broad maxima like that produced by a melted molecular substance. The character of the scattering pattern would be controlled entirely by F , which we have not considered in this discussion. Finally, what if there were some disorder in the crystallite assemblage? Depending on the nature of the disorder and the symmetry of the structure, some spots would be extended in one or more of the three dimensions, others would be unaffected, and additional diffuse spots would appear between the spots in some of the rods. The amounts of these changes would depend on the extent of the disorder. What if the crystals were reasonably large in the X and Y dimensions, but were only one unit cell thick along Z ? Then, the vertical arrays of spots shown by Figs. 10.1 and 10.2 would be drawn out into rods or pillars of continuous intensity along Z^* , modulated only by slow changes in F along Z^* . This is the turbostratic condition, which is discussed next.

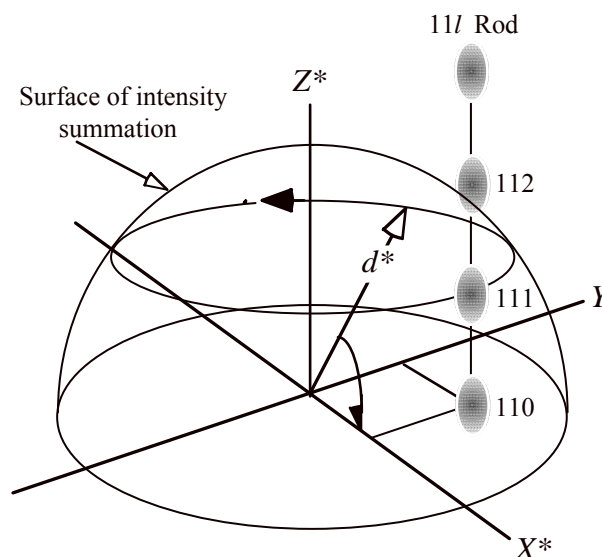


Fig. 10.2. Intensity summation in three-dimensional reciprocal space for the intensity of diffraction from a set of $11l$ planes in a randomly oriented powder.

TURBOSTRATIC DISORDER

Theory

This type of disorder is present in almost all smectite minerals. The 2:1 silicate layers are stacked along the normal to $d(001)$ so that no layer is tilted with respect to that line, but the layers are displaced from each other in the X - Y plane by random amounts and are rotated about the normal by random amounts. Imagine carelessly tossing playing cards one by one onto a pile on a flat surface. If the cards represent the 2:1 layers, the pile is a turbostratic “crystal,” or at least it acts like a crystal with respect to the basal X-ray reflections. Figure 10.3 shows such an arrangement. This structure is not possible with the micas or chlorites because the interlayer ions or hydroxide

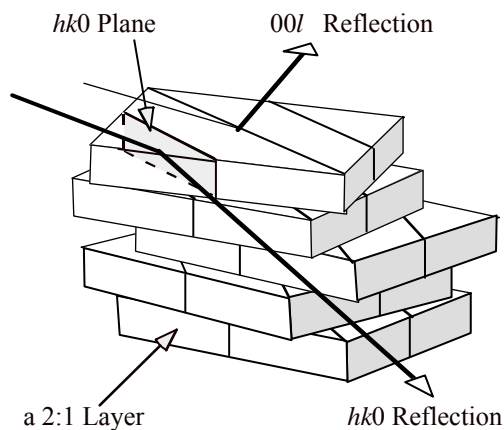


Fig. 10.3. Turbostratic stacking of 2:1 layers.

structure key adjacent layers into repeatable and fixed positions. But the weakly bonded exchangeable cations in the smectites evidently force no such ordering.

Let's rotate the turbostratic crystal of Fig. 10.3 about an axis perpendicular to the layers and try to get diffraction from a set of prismatic planes like the $hk0$ (Fig. 10.3). Diffraction will take place if the layer on the top is aligned suitably with respect to the incident beam. But the other four layers cannot diffract from this same plane because their orientations do not coincide with that of the top layer. In fact, in this example, no orientation of the

crystal can produce $hk0$ (or hkl) reflections from more than one layer. The other layers might as well not be there, as far as the diffraction process is concerned. With respect to the $hk0$ plane, we say that the layers are optically incoherent with respect to each other, and a randomly oriented aggregate of such crystals will produce hkl diffraction only from single layers. To calculate diffraction from the $hk0$ plane, you would set $N_3 = 1$ in Eq. (10.1). Note that the planes of the $00l$ series are optically coherent. Diffraction from them, given the proper angle of incidence, would be described by $N_3 = 5$ for Fig. 10.3.

Return to Fig. 10.1 and single out one of the vertical rows of spots, say the $20l$. We remarked earlier (p. 334) that the intensity of, for example, an $h0l$ reflection falls to zero along Z^* at the values $l_0 \pm 1/N_3$. This means that the intensity of the 202 spot falls to zero at the position of the 203 , and the 203 falls to zero at the position of the 202 spot. In between their positions they are additive, producing an intensity continuum between these two and by induction, between all spots in a row. In short, the spots of Fig. 10.1 are drawn out into vertical rods along Z^* whose vertical intensity changes slowly with l according to Eq. (10.2), as has been noted earlier. The diameter of the rods, *i.e.*, their X - Y cross section, is controlled by the X - Y dimensions of the crystals [N_1 and N_2 in Eq. (10.1)].

X-ray diffraction requirements for three-dimensional optical coherence are very strict, and disorder need not be nearly as drastic as that shown by Fig. 10.3. For crystals that average a few hundred Å in the X and Y directions, random rotations of only half of a degree produce fully turbostratic diffraction patterns.

The reciprocal space construction is the easy way to visualize the origin of the two-dimensional diffraction band that identifies turbostratic disorder. Our development is taken from Brindley (1980). You might want to read his treatment if we leave you with any confusion. Figure 10.4 serves as the basis of the discussion. Shown are the familiar (by now) reciprocal space coordinates and a single rod for a turbostratic structure. The series of

concentric arcs depicts a sequence of values of d^* (or 2θ) over which the intensity is summed. These are numbered to establish correspondence with the diffraction profile of Fig. 10.4B, which is diagrammatic only. Start with arc 1 and imagine integrating the intensity along its length. Only the left edge of the rod is intercepted, so the intensity is very weak for this value of d^* . Arc 2 cuts down through a significant portion of the rod, and its path almost intersects the center, where the intensity is greatest. The resulting intensity is sharply increased, causing the characteristic step rise on the low-angle side of the developing two-dimensional reflection or band. Arc 3 cuts most of the way through the rod and has the longest path length through it. It produces the maximum intensity. The remaining arcs produce continuously diminished intensity because they pass through the rod at angles that are progressively nearer to 90° , which would give the minimum arc in F .

The shape of the band is modified if changes are taken into account along Z^* . In extreme cases, a rapid diminution of F along Z^* causes the asymmetric tail of the band to be reduced, giving rise to a quite symmetrical peak that appears to be a legitimate three-dimensional reflection. Such an example is the 02; 11 band for the micas at about $d = 4.5$ Å. Brindley (1980) shows numerous calculated examples of the effect of F on band shapes.

Two-dimensional bands such as the one illustrated by Fig. 10.4B occur at diffraction angles corresponding to $h00$, $0k0$, and $hk0$ reflections. Three-dimensional peaks (h , k , and $l \neq 0$) are missing, and their positions lie in the tails of the two-dimensional bands. A word of caution: The intensity maximum of the band does not necessarily coincide with d for any specific reflection such as the 020, and this can cause difficulties in the measurement of $d(060)$, which is commonly used to estimate the b dimension.

Random powder XRD studies of smectite, I/S, and illite can be profitably restricted to the angular range $2\theta = 16^\circ$ to 44° because this range contains all

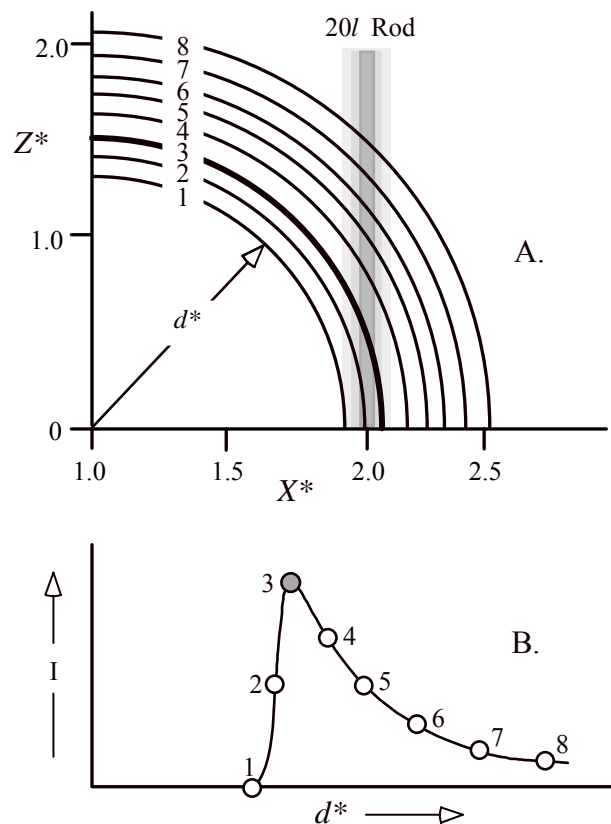


Fig. 10.4. Summation arcs in reciprocal space (A) and the development of a two-dimensional diffraction band (B).

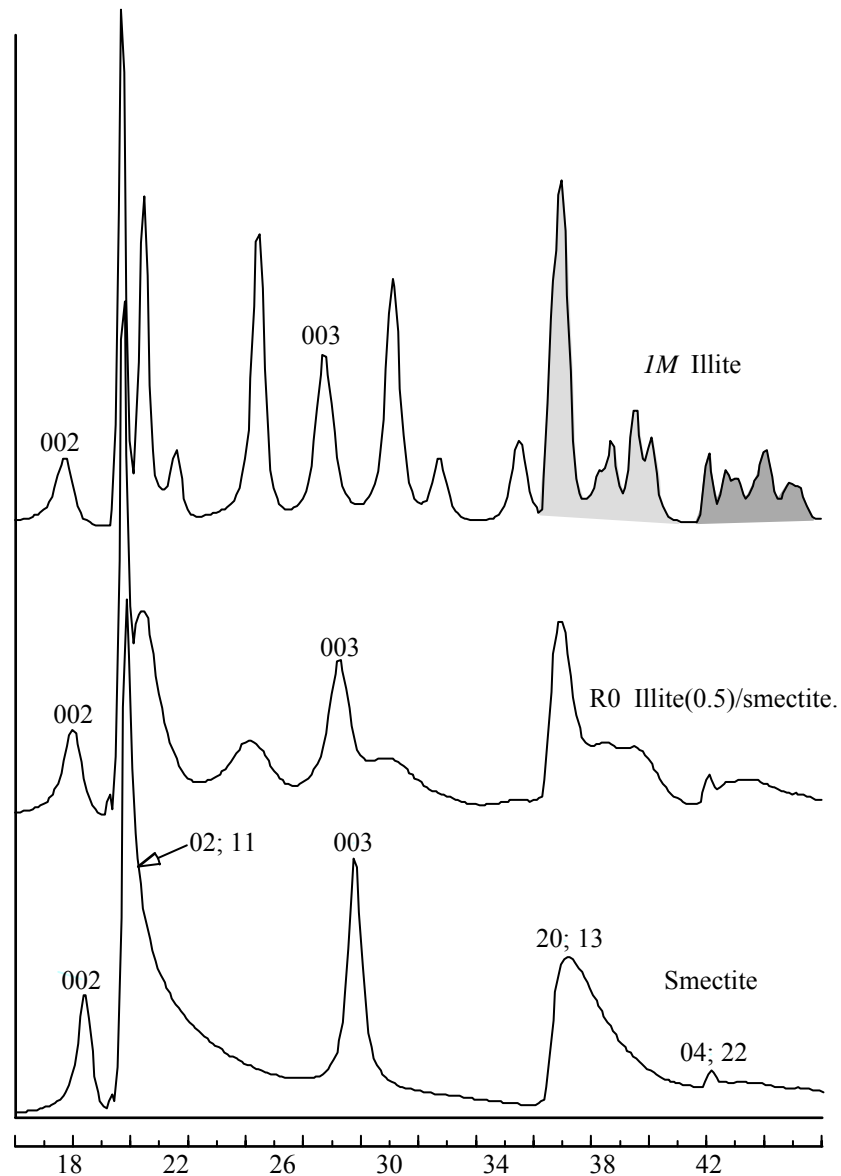


Fig. 10.5. Fully turbostratic smectite, partially turbostratic I/S, and defect-free *IM* illite. Unshaded regions contain peaks for which $k \neq 3n$, $k = 3n$ reflections are lightly shaded, and dark shading depicts mixed peak types.

the strong nonbasal reflections, with the exception of the 060, that collectively provide the most diagnostic information on the kinds and extents of disorder present. Remember, basal peaks will be present too; so in the case of I/S, it is desirable to simplify the basal pattern so as to minimize interferences from the $00l$ series. This is best done by dehydration, and that procedure was described in Chapter 6.

Smectite

A diffraction pattern for a turbostratic smectite is illustrated in Fig. 10.5. The

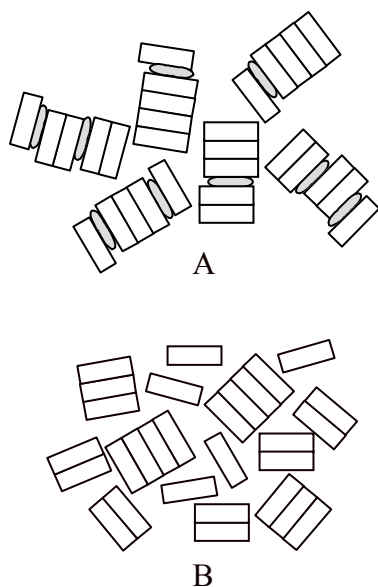


Fig. 10.6. Randomly oriented MacEwan crystallites (A) and their illite particles (B).

crystallite dimensions are $N_1 = 60$, $N_2 = 30$, and $N_3 = 1$ (Eq. 10.1) for the hk pattern and a distribution of values for $N_3 = 1$ to 30 for the basal series assuming a dehydrated preparation [$d(001) = 9.7 \text{ \AA}$]. The two-dimensional diffraction bands are labeled with hk because for $N_3 = 1$ there can be no integral l component in the diffraction peaks. The calculated pattern includes the effects of the structure factor, and these cause the markedly different shapes of the three bands. Examination of the smectite pattern of Fig. 10.5 leads to the conclusion that the 20; 13 band is the best to use for detecting (and quantifying, as we will see later) turbostratic disorder. This band is intense compared to the 04; 22 band and much more asymmetrical than the 02; 11. Also shown in Fig. 10.5 for comparison is a IM structure containing a significant portion of turbostratic disorder (middle trace) and a defect-free IM illite (top trace).

Illite/Smectite

Mixed-layered illite/smectite contains 2:1 illite layers that are in perfect juxtaposition because the surface structure of the layers is keyed on the interlayer K. Experimental evidence published by Reynolds (1992) and other unpublished data indicate that the expandable, or smectitic interlayers, are not keyed; they are sites of turbostratic defects. Figure 10.6A is a cartoon of a few MacEwan crystallites of the many that make up a crystalline aggregate that we call a specific I/S. These are shown diagrammatically in random orientation. The question is, how do they diffract? The $00l$ series is the well-known irrational pattern described and discussed in Chapter 8. But the three-dimensional reflections are identical to those produced by a random arrangement of separated illitic crystallites (Fig. 10.6B). This behavior is caused by the nature of turbostratic defects that break the optical coherence of the MacEwan crystallites and cause the nonturbostratic fragments to diffract like separate crystallites. You might say that quartz and feldspar crystals in a powder aggregate are separated by turbostratic-like interfaces and that is why you get the simple sums of their diffraction patterns, and not a mixed-layered quartz/feldspar pattern. These illitic fragments are the fundamental particles of Nadeau et al. (1984), and, to use their terminology, the fundamental particles show interparticle diffraction for the $00l$ series, but not for three-dimensional reflections.

I/S has an incidence of turbostratic defects that is proportional to the percent expandability or smectite content of the species (Reynolds, 1992).

The I/S series thus separates the end members of (1) pure illite with no turbostratic defects, and (2) pure smectite with turbostratic defects separating each 2:1 layer. The middle trace of Fig. 10.5 represents R0 illite(0.5)/smectite, and here is how it was calculated. The statistical distribution of MacEwan crystallites for this species was calculated, and the numbers of 1, 2, 3, etc. unit-cell-thick illite particles were summed for all the crystallites in the assemblage, producing a synthetic particle-size histogram of the type measured by Nadeau et al. (1984), who used transmission electron microscopy. We assumed here that the internal stacking was *IM*, and the three-dimensional diffraction pattern was computed by this distribution of illite crystallites. The excellent agreement that this procedure gives with respect to real samples, for which the illite content is known from the *00l* patterns, is shown by numerous examples in Reynolds (1993) and McCarty and Reynolds (1995).

If you compare the three traces in Fig. 10.5, you can see the deterioration of the three-dimensional peaks caused by increased expandability. Figure 10.7 shows a calculated series of profiles that demonstrate the effects of increased turbostratic character on the *20l*; *13l* diffraction region. You could estimate percent expandability by analyzing the shapes of the *20l*; *13l* profiles from experimental samples, but it is easier and more accurate to base your interpretation on the *00l* series.

The illitic fundamental particles in I/S could be internally stacked according to any of the mica polytype schemes, but the evidence so far suggests that they are always stacked in the *IM* or *IMd* arrangement. You might think, “So, I/S is a *IM* illite structure that contains some turbostratic defects, and that is what is meant by the term *IMd*.” Unfortunately, many would agree with that reasoning. Such a mineral is indeed a disordered *IM* structure, but that is not the meaning of the term *IMd* as used by, for example, Smith and Yoder (1956), Méring (1975), and Bailey (1988). We need help here from the International Committee on Nomenclature! In this book, we follow the authors cited who used the term “*IMd*” to denote the *IM* structure disordered by randomly distributed $n120^\circ$ and $n60^\circ$ rotations. Turbostratic stacking, small crystallite size (which is really the same thing—the lower limit being crystallites one unit cell thick), mixed-layering, and poorly identified “poor crystallinity” do not qualify for our use of the “*d*” in *IMd*.

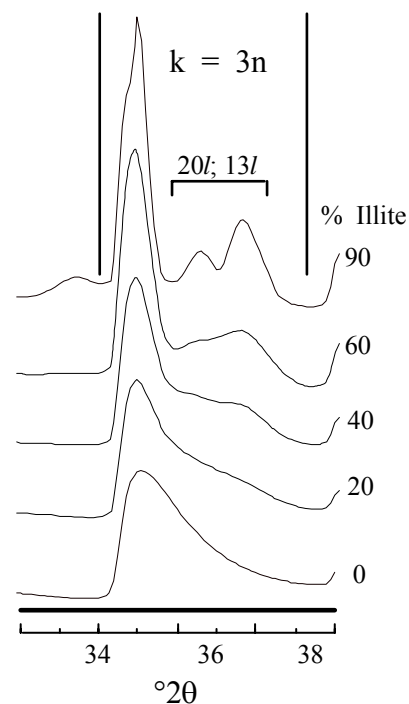


Fig. 10.7. The *20l*, *13l* diffraction region and the affects of turbostratic stacking that accompanies expandability in I/S.

Rotational Disorder in Illite and Illite/Smectite

Layer rotations that are integral multiples of 60° ($n60^\circ$) or 120° ($n120^\circ$) affect only some of the hkl reflections. Distortions of the surface oxygen planes in the dioctahedral micas produce a plane with trigonal symmetry; and for the trioctahedral types, the octahedral cation sheet is also trigonal. Trigonal symmetry has a 3-fold axis of rotation, so rotations of 120° or 240° have no effect on some of the atomic patterns. Other aspects of the mica structure are not trigonal, so $n120^\circ$ and $n60^\circ$ rotations do cause changes in a crystal's diffraction pattern. Méring (1975) has used the term *semiordered* for mica structures with randomly distributed $n120^\circ$ rotations. The prefix *semi* means that this type of disorder destroys only some of the hkl reflections; planes unaffected by $n120^\circ$ rotations may continue to diffract; for these, there is no disorder.

The point comes up: How d is IMd ? You can visualize a complete series that covers the range between a pure IM structure and one that is totally disordered; and indeed, members of such a series are present in nature, although they have been previously identified only as either IM or IMd . We define the location of a structure in that series by the variable P_0 , which means the probability of a zero-layer rotation with respect to the layer below it along Z . For the case of $n120^\circ$ rotations, and defining P_{120} and P_{240} in a fashion identical to P_0 ,

$$P_0 + P_{120} + P_{240} = 1 \quad (10.3)$$

and

$$P_{120} = P_{240}$$

i.e., rotations of 120° and 240° , with respect to the underlying layers, are crystallographically equivalent operations so that there is no tendency for one to be more likely than the other. If $P_0 = 1/3$, then all rotations are equally probable, and we take this as the extreme case of disorder. $P_0 = 1$ describes the end-member IM structure.

The disordered case brings up an interesting point. One could look at IMd as disordered $2M_1$ ($2M_{1d}$) because plus and minus 120° rotations are as common as any other pair. Perhaps it is a $3Td$ because the spiral axis caused by 120° - 120° - 120° -etc. rotations are also represented. Bailey (1988) suggested that we call the totally disordered case simply Md because the layers are certainly monoclinic and they are stacked in a disordered fashion. We like this idea but retain the older nomenclature because this change has not been formally sanctioned.

We must delve deeply into the crystallography of the micas to see why these strictly defined layer rotations produce the diffraction results that they do. The shape of the illite (or mica) unit cell is very nearly orthohexagonal. This means that the lattice has only a slightly deformed hexagonal pattern.

But the symmetry of the unit cell is monoclinic. The shape and dimensions of the unit cell dictate at what diffraction angles the hkl reflections occur, and their intensities are determined by the occupants of the atomic positions that fix the symmetry of the cell and manifest themselves in the structure factor F_{hkl} . Perfect orthohexagonality is present if the following relations hold.

$$b = a\sqrt{3} \quad (10.4)$$

and

$$c\cos\beta = -a/3 \quad (10.5)$$

where a , b , and c are the unit cell dimensions and β is the monoclinic angle. The relation of Eq. (10.5) means that the top oxygen plane of the 2:1 layer is translated in the $-X$ direction with respect to the upper oxygen plane of the underlying layer by an amount that is equal to $1/3$ of the a dimension. The ideal monoclinic angle is $\beta = 99.8^\circ$ for a $d(001)$ value of 10 \AA , characteristic of the micas, and $a \blacktriangleright 5.2 \text{ \AA}$ and $b \blacktriangleright 9.0 \text{ \AA}$, which are also characteristic of micas and almost always perfectly orthohexagonal. If we compare ideal β with the muscovite or illite value of $\beta = 101.3^\circ$, we see that there is some overshoot that has displaced the top oxygen plane a bit more than is ideal. This is mostly caused by the larger octahedral site at the vacant cation location that lies on the M1 position in the X - Z plane. Consequently, the muscovite-like illite layer is not perfectly orthohexagonal, but it is close enough to make the following discussion applicable.

Figure 10.8 shows two illite unit cells, the uppermost of which has been rotated by 120° with respect to the bottom one. The bold arrows indicate the $-X$ directions for each cell. The axis of rotation is normal to $d(001)$ and passes through the center of the K atom that lies in the interlayer plane that separates the two cells. This figure is not a cartoon—it has been accurately scaled. The lower cell has marked on it the (200) plane, and the upper cell has a trace of a member of the $(\bar{1} 31)$ set. Note that orientation of the (200) plane of the lower cell is coincident with the $(\bar{1} 31)$ plane of the upper cell. Therefore the 2 planes are in optical continuity. Furthermore, $d(200) = d(\bar{1} 31)$, and the intensities $|F(200)|^2$ and $|F(\bar{1} 31)|^2$ are equal except for multiplicity. In short, the intensity of the 200 reflection from a crystal is unaffected by layer rotations of 120° (or 240°).

Consider now a different reflection like the 020 (Fig. 10.9). A 120° rotation has indeed aligned the projections of the (11 l) and (020) planes on the X - Y interface, but no integral or near-integral value of l produces coincident orientation in three-dimensional space between the (020) and any (11 l) plane. Optical continuity between the two unit cells is lost for this arrangement, and there would be no 020 or 11 l reflections.

The different geometries demonstrated by Figs. 10.8 and 10.9 can be

extended to a general rule. All reflections for which $k = 3n$ are unaffected by 120° or 240° rotations ($k = 0$ counts as a $3n$ reflection). Reflections for which $k \neq 3n$ will be missing or broadened, depending on the incidence of rotations. The situation for $n60^\circ$ rotations is more complicated.

Figure 10.10 shows a calculated powder diffraction pattern for a *IM* illite. The top trace is the entire pattern, and the bottom one shows the high-angle region in more detail. The peaks are labeled, and their indices demonstrate that for the *IM* illite space group ($C2/m$) reflections are limited to those for which $h+k$ is an even number. Ignore the $00l$ series, which gets in the way but tell us nothing about rotational disorder, and you can see that the pattern can be divided into three regions. Between 19° and $34^\circ 2\theta$, all the peaks are of the type $k \neq 3n$. Specifically, they are the $11l$ and $02l$ reflections. Between 34°

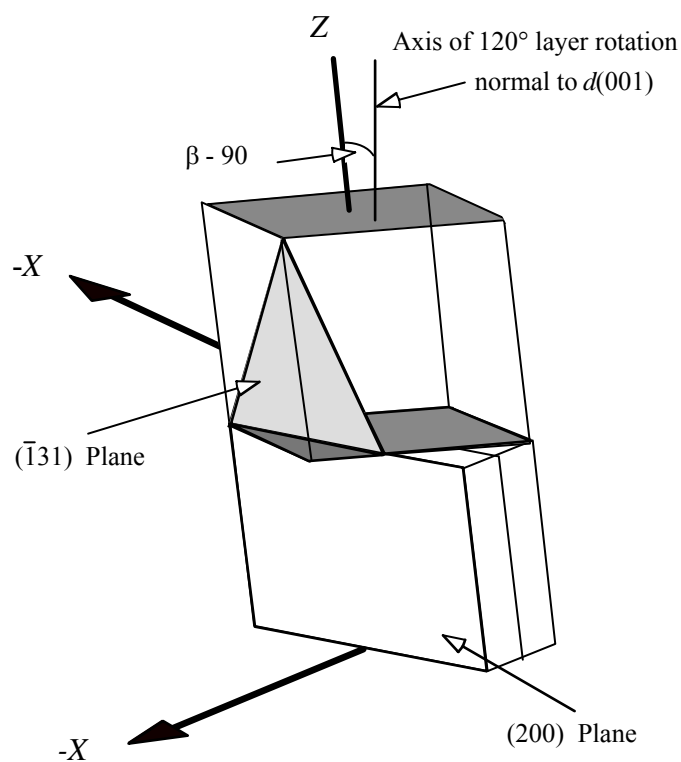


Fig. 10.8. Coincidence of the (200) and $(\bar{1}31)$ planes caused by a layer rotation of 120° ($-X$ axis of upper unit has rotated 120° from that of the lower $-X$ axis).

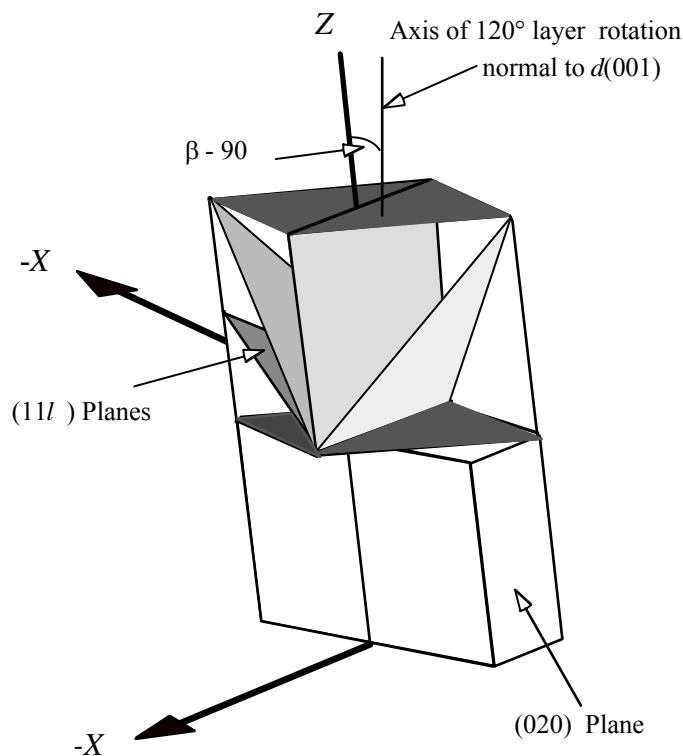


Fig. 10.9. A rotation of 120° produces no coincidence between the (020) plane with any member of the (11 l) series.

and 39° , they are $k = 3n$ types (20 l and 13 l). From 39° 2θ to 44° , the reflection types are mixed. From what you have learned, you can conclude that the low-angle region will be affected by rotational disorder, and the intermediate 2θ range will not. The higher-angle range, which fortunately contains only weak peaks anyway, will show complicated changes if rotational disorder is increased.

Turbostratic stacking affects *all* the peaks, so it is a simple matter to distinguish it from rotational disorder. Figure 10.11 demonstrates the principles described above. In both patterns, the 11 l ; 02 l reflections are weak and broad, attesting to some kind of disorder. The I/S (upper trace) shows a poorly modulated 20 l ; 13 l profile because interstratification with smectite has introduced many turbostratic stacking defects. The lower trace represents an illite in which rotational disorder has broadened the 11 l ; 02 l peaks so that they resemble those in the I/S pattern; but the $k = 3n$ angular region has well-developed peaks because 120° and 240° rotations do not affect them. The similarities of the $k \neq 3n$ peaks for the two are remarkable.

We need to discuss rotational disorder and the $k \neq 3n$ peaks—a subject that penetrates to the heart of the meaning of such disorder. We know that turbostratic defects resulting from mixed-layering cause the $k \neq 3n$ spots, as well as the $k = 3n$ spots, to be extended toward the shape of pillars of nearly

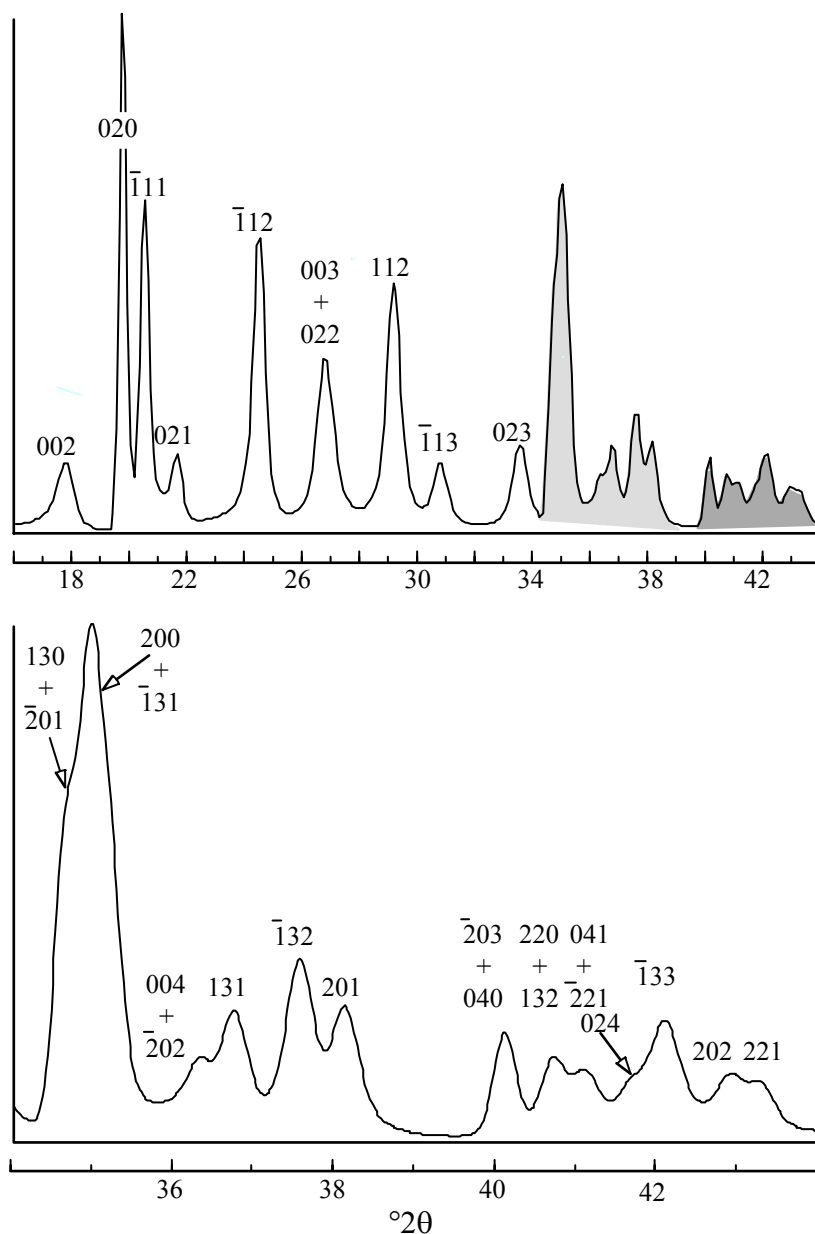


Fig. 10.10. Calculated random powder diffraction pattern of *IM* illite. Unshaded regions contain peaks for which $k \neq 3n$, $k = 3n$ reflections are lightly shaded, and dark shading depicts mixed peak types. The lower tracing is an expansion of the high-angle region of the upper tracing.

constant intensity along Z because if the crystal is only one unit cell thick, there can be no three-dimensional Bragg diffraction. Is the same principle operating for the rotationally disordered condition? No, the $k \neq 3n$ rods are essentially pillars of uniform intensity for a very different reason. No single crystallite can represent a rotationally disordered illite. There is no such thing as a representative crystallite. The diffraction pattern from a *IMd* specimen is the sum of the *intensities* of very many crystallites with different stacking

sequences whose abundances are determined by the statistics of the composition. If $P_0 = 1/3$, then all rotations are equally probable, and the crystallite assemblage contains individuals that consist of $1M$, $2M_1$, $3T$, and other polytypes not found in nature such as $3M$, in addition to sequences too long to repeat within the crystallite thickness. These produce reciprocal lattice spots all along the $k \neq 3n$ rods at values of l different from the $1M$ positions, and there are so many of them that the rods approach a condition of constant intensity along Z^* . For example, a $2M_1$ stacking sequence produces spots midway between the $1M$ spots, and a $3T$ generates two spots between each $1M$ reciprocal lattice node.

Figure 10.12 illustrates the character of the diffraction patterns for the range $1M$ to $1Md$. The $k \neq 3n$ reflections behave as expected, but the $k = 3n$ region shows some changes despite what we said earlier, namely, that the $k = 3n$ reflections should not be affected by $n120^\circ$ rotations. The changes in these

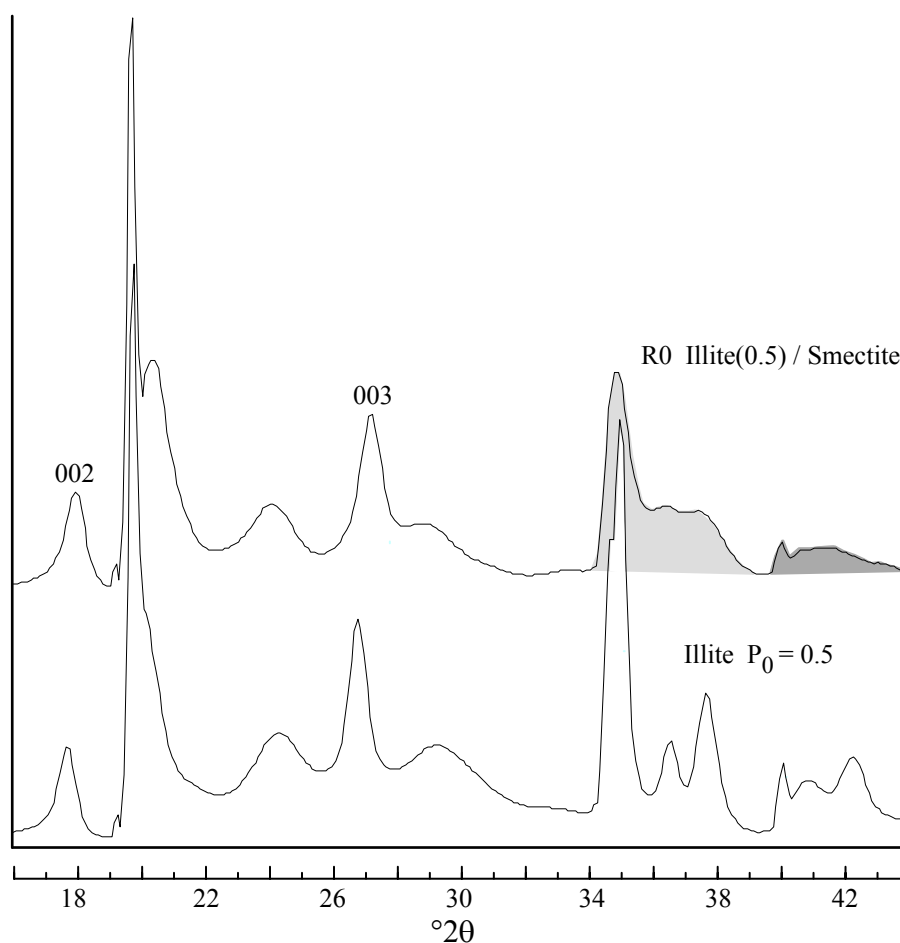


Fig. 10.11. Two kinds of disorder, rotational ($P_0 = 0.5$) and turbostratic (mixed-layering), and their manifestations in powder diffraction patterns. Unshaded regions contain peaks for which $k \neq 3n$, $k = 3n$ reflections are lightly shaded, and dark shading depicts mixed peak types.

diffraction profiles occur because the *IM* layer is not perfectly orthohexagonal; its monoclinic angle is 101.3° instead of the ideal value of 99.8° . These reflections provide a very important diagnostic parameter; if you can see any separation of the two peaks between 36° and 38° into four components, as in the top tracing, the structure has very little disorder and rates the name *IM*. An examination of the literature suggests to us that earlier studies would have categorized the top three traces as *IM* despite the disorder present. Clay mineralogists have yet to correlate decreasing rotational disorder with any geologic parameter.

Bailey (1975) has observed that $n60^\circ$ rotations are uncommon in the

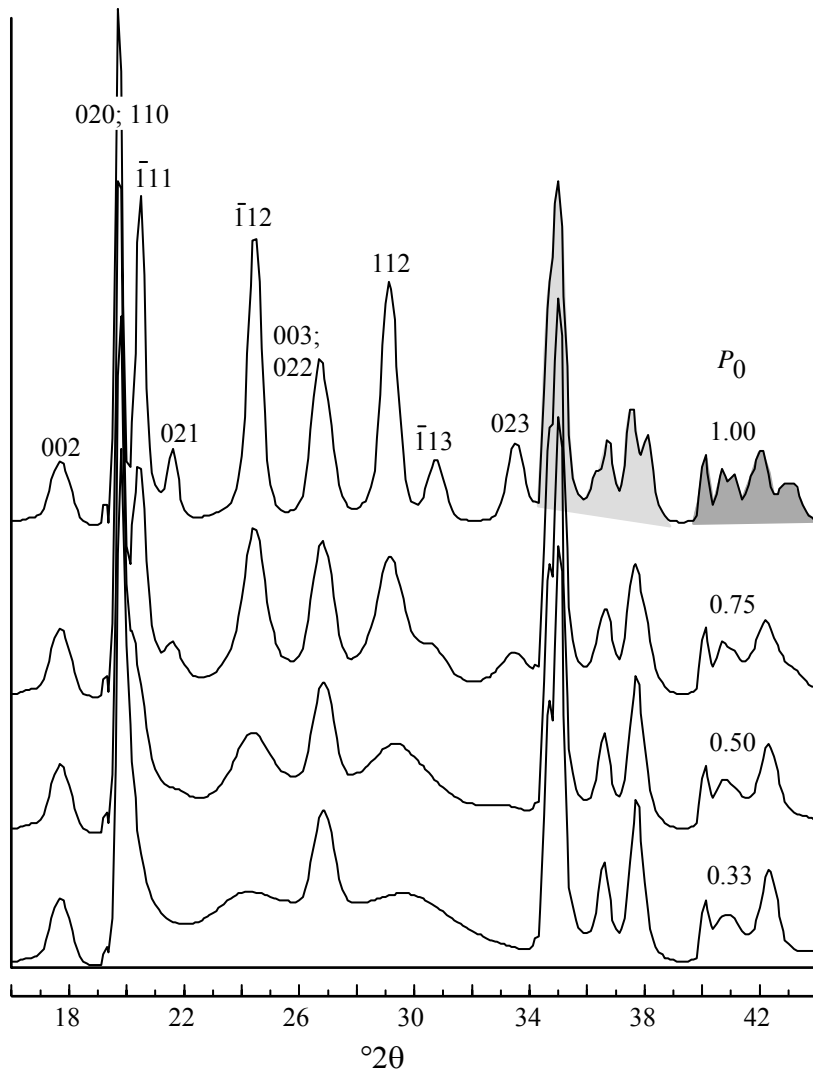


Fig. 10.12. Calculated diffraction patterns for the series *tv-IM/tv-IMd* illite. Unshaded regions contain peaks for which $k \neq 3n$, $k = 3n$ reflections are lightly shaded, and dark shading depicts mixed peak types. P_0 is the probability of a zero-layer rotation with respect to the layer below it along *Z*.

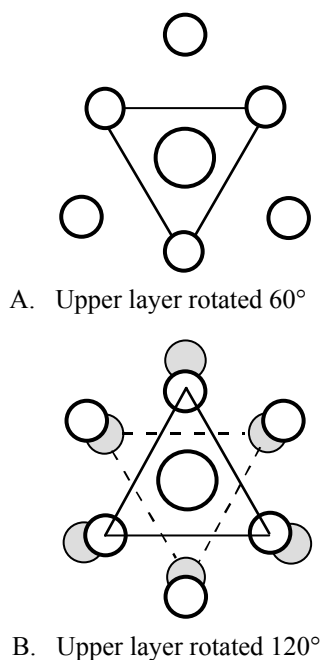


Fig. 10.13. Ditrigonal (A) and octahedral (B) oxygen coordination about interlayer potassium in illite. Shaded atoms represent oxygen atoms in the lower plane.

dioctahedral micas, the best-known example of which is the rare $2M_2$ polytype. He suggests that the reason is that the oxygen coordination about the interlayer potassium is energetically unfavorable. Figure 10.13 demonstrates the differences between 60° and 120° rotations. Diagram A shows that the upper and lower atomic planes are exactly superimposed, leading to ditrigonal coordination of oxygen about potassium. This arrangement brings the upper and lower oxygen atoms in close proximity, causing repulsive forces to destabilize the structure. Figure 10.13B depicts a 120° rotation. Shaded atoms represent oxygen atoms in the lower plane. The lower and upper oxygen triangles form octahedral coordination about potassium and maximize the separation of oxygen atoms in the upper and lower planes, leading to a more stable configuration.

McCarty and Reynolds (1995) found $n60^\circ$ disorder in detectable amounts in Paleozoic K-bentonites (I/S). Correlations with chemical composition suggest that $n60^\circ$ disorder increases with octahedral substitution of Mg for Al (and less Al for Si in the tetrahedral sites), such as occurs in the mica end member celadonite. Interesting partial corroboration of this conclusion is provided by the results of Sakharov et al. (1990), who reported that disorder in glauconite is dominated by $n60^\circ$ rotations. The common wisdom is that glauconite tends to be more celadonitic than illite.

Rotations of $n60^\circ$ and $n120^\circ$ have different effects on diffraction patterns. For the former, reflections of the type $k = 3n$ have no coincident planes across the interfaces between such rotations, unlike the case for $n120^\circ$ rotations. So we expect, and do see, changes in the region between 34 and $39^\circ 2\theta$ that accompany $n60^\circ$ disorder, changes greater than those shown in Fig. 10.12. Figure 10.14 shows calculated patterns for partially disordered *IM* structures ($P_0 = 0.7$) in which the proportion of $n60^\circ$ rotations varies from none ($P_{60} = 0$ and therefore the remaining 0.3 of rotations are all $n120^\circ$ rotations) to the end member case in which the proportions of 0° , 60° , 180° , and 300° rotations are equal ($P_{60} = 1$). The tendency of this type of disorder is to coalesce the two “double” reflections into a single maximum. The most sensitive indicator for $n60^\circ$ disorder is the lack of separation of these two peaks.

The effects of $n60^\circ$ rotations on the $k \neq 3n$ diffraction pattern are complicated because 60° , 180° , and 300° rotations produce dissimilar results, and each influences some but not all the reflections. Because some of them are unaffected (like the case of $n120^\circ$ rotations on the $k = 3n$ peaks), the $k \neq 3n$ diffraction region will appear to be somewhat less disordered than would be the case for rotations of $n120^\circ$ (as in Fig. 10.12).

Cis-Vacant Illite and Interstratified Cis- and Trans-Vacant Illite/Smectite

We have described in Chapter 4, Fig. 4.3, two kinds of illite unit cells, the centrosymmetric and well-known *trans*-vacant (*tv*) variety and the newly (in illite) recognized *cis*-vacant (*cv*) noncentric structure. Our knowledge of *cv* structures is due to Russian scientists, particularly V. A. Drits and his colleagues. Tsipursky and Drits (1984) reported that many dioctahedral smectites have this structure, and Drits et al. (1984) derived the unit cell and atomic parameters for *cv* illite and published calculated diffraction patterns for it. Zvyagin et al. (1985) first reported a *cv* illite, and Reynolds and Thomson (1993) and Drits et al. (1993) described other occurrences. McCarty and Reynolds (1995) showed that many Paleozoic K-bentonite I/S minerals have illitic portions that consist of randomly interstratified *cv* and *tv* layers. They are not simply I/S, but interstratified *tv*-illite/*cv*-illite/smectite. Quantification of such structures requires comparisons of experimental with calculated diffraction patterns such as those produced by WILDFIRE[©] or one of the Russian programs.

Figure 10.15 shows experimental diffraction patterns of *tv* and *cv* illite. The *tv* specimen is a hydrothermal sericite provided by D. D. Eberl, and the *cv* example is the illite from the Potsdam sandstone described by Reynolds and Thomson (1993). Reflections from the same *hkl* planes are at measurably different diffraction angles because the *cv* variety has $\beta = 99.3^\circ$ and for the *tv* cell, $\beta = 101.3^\circ$. $\beta = 99.3^\circ$ also gives a “cleaner” $k = 3n$ diffraction profile because it is close to the ideal orthohexagonal value of 99.8° . You should have no trouble telling these two structures apart. The four $11l$ peaks of almost equal intensity are the diagnostic *cv* illite signature. We are confident that many occurrences of *cv*-illites will be documented if you students out there will take the trouble to achieve random orientation for your samples and get high-quality powder diffraction patterns from the many illites that you will see as clay scientists. The resulting database will (we hope, with the usual scientific optimism) finally make it possible to assign specific geologic conditions to the occurrences of this “new” structure. Analyses of more than 100 K-bentonites, including some published by McCarty and Reynolds (1995), the report of Lee et al. (1995) of large amounts of *cv* *IM* illite in sandstones of poor reservoir quality, and other as yet unpublished work, lead us to conclude that for these rocks, the *cv* variety is far more abundant than the *tv* species.

There is a disquieting circumstance in this otherwise optimistic picture.

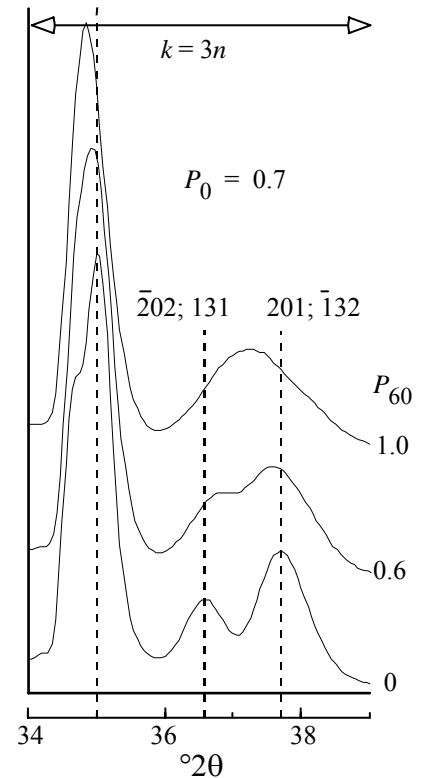


Fig. 10.14. The effects of $n60^\circ$ rotations on the $k = 3n$ reflections 34 to $39^\circ 2\theta$.

Recall that the *cv* variety is almost perfectly orthohexagonal. Well, the *3T* mica polytype is indeed hexagonal; consequently, both structures produce almost identical peak positions. By nasty chance, even the intensities of the reflections from the two are very similar. Reynolds and Thomson (1993) were able to resolve this difficulty by showing that, within the accuracy of measured peak positions, their data fit the monoclinic *cv* structure better than they accommodate the *3T* type. But if there is rotational disorder, or interstratification with *tv* layers, you might not be able to measure peak positions with sufficient accuracy to confidently exclude the *3T* interpretation. The differentiation would be simple by single-crystal methods, but they are not likely to be of much help with clay-sized crystallites. Discrimination can be accomplished by oblique-texture electron diffraction, but despite its long-

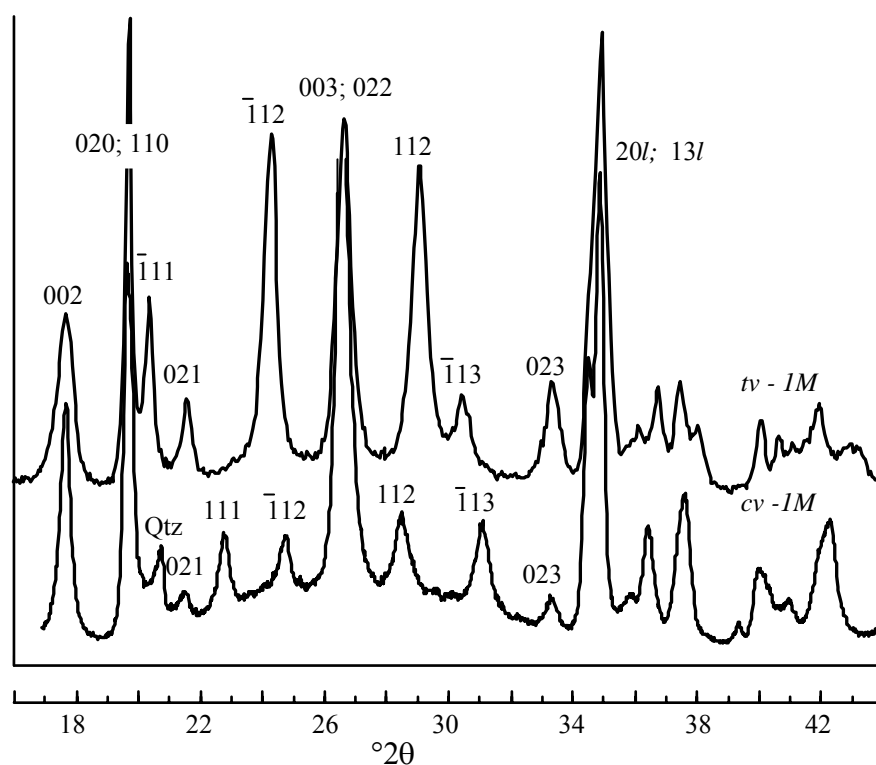


Fig. 10.15. Experimental powder diffraction patterns of *cv*- and *tv*-illite. Note the diagnostic (111) peaks.

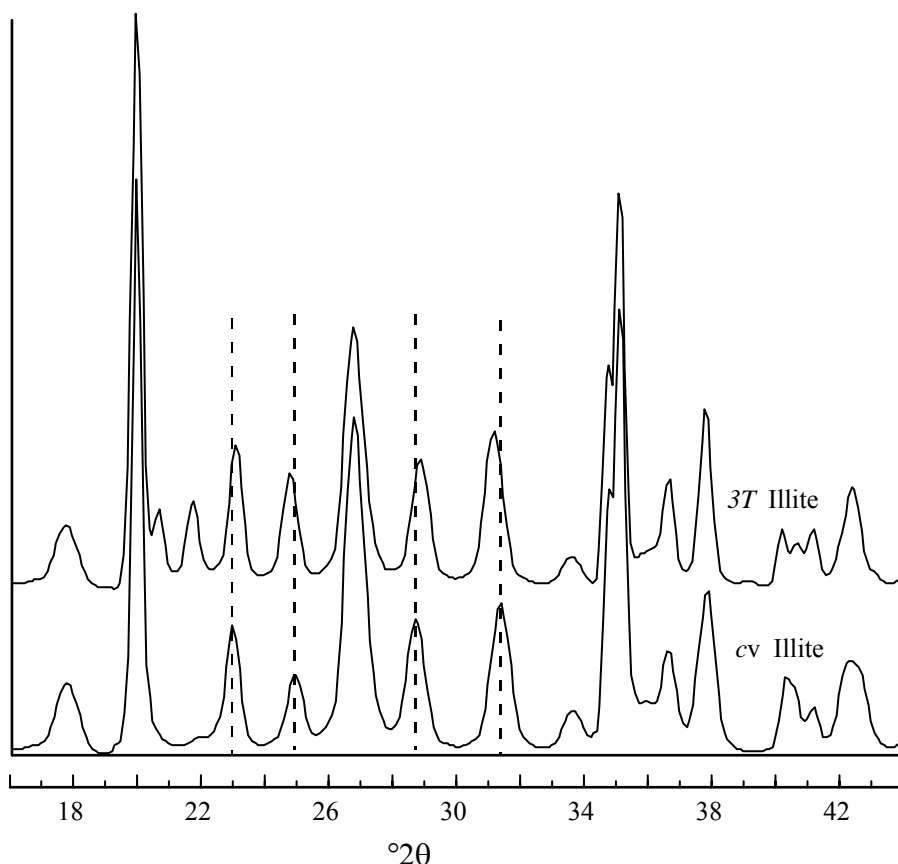


Fig. 10.16. Calculated powder diffraction patterns of *3T tv*-illite and *IM cv*-illite.

term use and development by Zvyagin and his colleagues, it is a relatively unfamiliar technique outside of Russia. The problem is illustrated by Fig. 10.16. Where does this leave us? There is a lot to do on the subject of *cv* illite. But we will assume that the “new” structure is the *cv* variety, not the *3T* polytype, as we go on to discuss its diffraction characteristics in disordered and interstratified structures.

A series of calculated patterns for interstratified *cv/tv* illite is portrayed in Fig. 10.17. The end members have been omitted to simplify the graphics, but that omission is not critical because you would be hard pressed to confidently identify 20% or less of either component in the other. We define P_{cv} as the decimal fraction of *cv* layers in the interstratification. Diagnostic features for the interpretation of *cv/tv* interstratification are (1) a shift in the positions of the 112 and $\bar{1}$ 13 reflections with changes in P_{cv} ; (2) appearance of the 111 peak at higher values of P_{cv} ; and (3) at large values of P_{cv} , four peaks of nearly equal intensity distributed in two pairs on opposite sides of the 003 illite reflection. The occurrence of the 111 is the crucial criterion. If you can see it at all, the structure contains at least 50% *cv* layers ($P_{cv} \geq 0.5$). Just to allay your suspicions that we are too carried away with synthetic data, we show on Fig. 10.18 some “real” examples taken from McCarty and Reynolds

(1995). These are I/S minerals from Paleozoic K-bentonites analyzed in the dehydrated condition. Note that they compare favorably with the calculated patterns on Fig. 10.17 except that some rotational disorder is present ($P_0 < 1$) and small amounts of smectite interstratification have introduced some turbostratic disorder. The $k = 3n$ region near $35^\circ 2\theta$ on the top trace shows some evidence of $n60^\circ$ rotational disorder (compare to Fig. 10.14).

A physical mixture of *cv* and *tv* types is easy to distinguish from an interstratified *cv/tv* structure for illites with little expandability and free from rotational disorder. The mixture will produce partially resolved reflections from each type, whereas the interstratification will yield peaks at intermediate

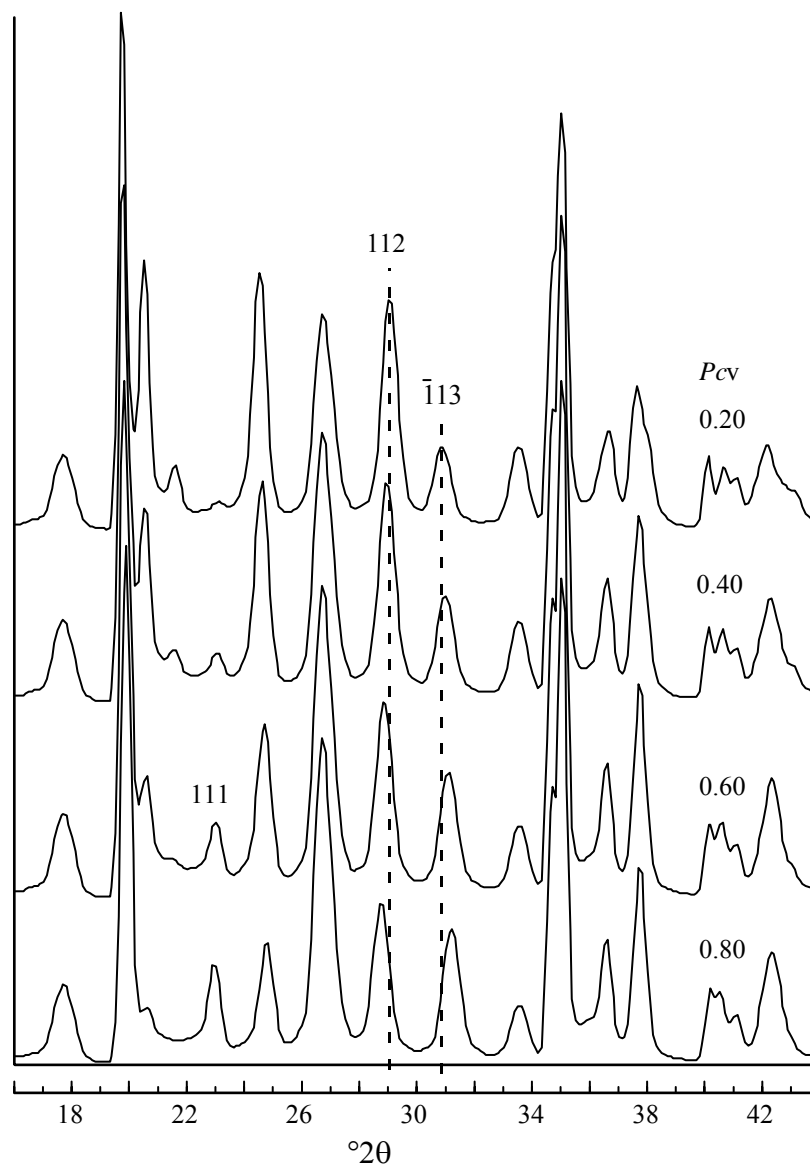


Fig. 10.17. Calculated diffraction patterns for interstratified *cv/tv* illite.



Fig. 10.18. Experimental diffraction patterns of I/S from Paleozoic K-bentonites (McCarty and Reynolds, 1995).

positions. V. A. Drits (personal communication, 1993) has pointed out that the 020; 110 doublet at about $19.9^\circ 2\theta$ is different for the tv and cv structures, as the calculated data in Table 10.1 demonstrate. The importance of this observation is twofold. A peak at 19.72° identifies the tv IM polytype, and a peak at 19.91° is diagnostic for the cv IM structure. Note that two peaks near 19.9° conclusively demonstrate the physical admixture of the two types of layers. Unfortunately, as rotational disorder increases, this discrimination cannot be made, and at some point it is impossible to distinguish a mixture from an interstratification. For the completely disordered case, $P_0 = 1/3$, there is little difference between diffraction patterns of the two cases. Figure 10.19 shows such a pattern for $P_{cv} = 0.6$, which is typical for many nonexpandable illites from shales. We have messed this pattern up a bit to better simulate experimental diffraction data. Some noise has been added, and a small degree of preferred orientation was introduced into the calculations. Does this common type of diffraction pattern mean that many IMd illites are interstratifications of cv and tv layers? Tune in in a few years and maybe we will know.

Figure 10.20 shows the effects of increasing $n120^\circ$ disorder on the

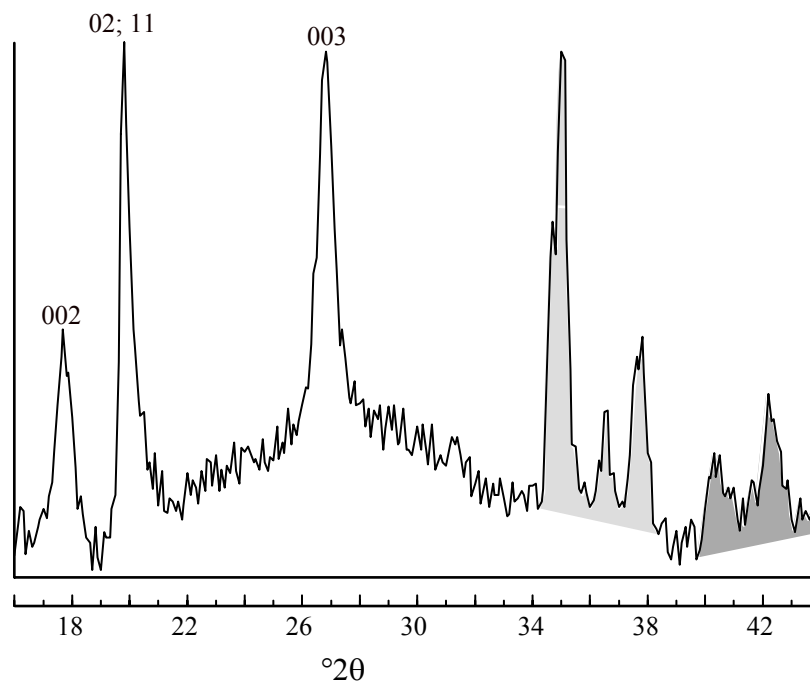


Fig. 10.19. Calculated diffraction pattern for completely disordered ($P_0 = 1/3$) interstratified *cv/tv* illite ($P_{cv} = 0.6$). Unshaded regions contain peaks for which $k \neq 3n$, $k = 3n$ reflections are lightly shaded, and dark shading depicts mixed peak types.

diffraction patterns of *cv IM* illite. As you would expect, the results are similar to those shown on Fig. 10.12 for the disordered *tv IM* series.

We close this chapter with an overview of the process of interpreting disorder by means of three-dimensional powder XRD patterns. Figure 10.21 illustrates the way to go about it. Figure 10.21A shows the diffraction angles that contain the $k \neq 3n$ reflections. The weak, broad $\bar{1}11$, $\bar{1}12$ and 112 reflections and the absence of the 111 peak should tell you that:

1. The layer structure type is *trans*-vacant *IM*, and
2. Disorder is present as evidenced by the breadths of the reflections.

The disorder could be turbostratic, caused by interstratification with smectite. Or it could be rotational stacking disorder due to $n120^\circ$ or $n60^\circ$

Table 10.1 Intensities and diffraction angles for the 020 and 110 reflections.

Peak	Intensity	d	2θ
<i>tv</i> 110	<1	4.44	20.01
<i>tv</i> 020	77	4.50	19.72
<i>cv</i> 110	79	4.46	19.91

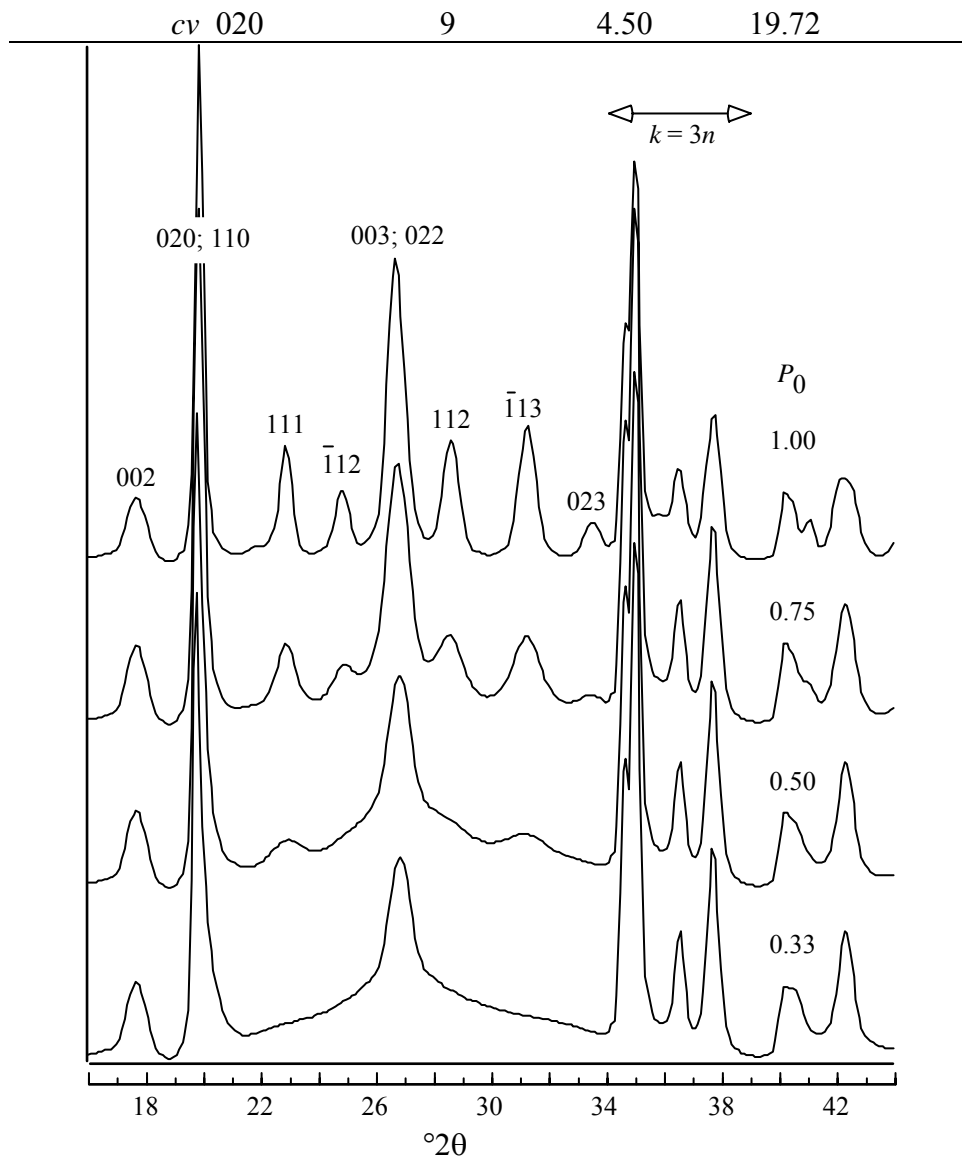


Fig. 10.20. Calculated diffraction patterns for the series *cv-1M/cv-1Md* illite illustrating increasing $n120^\circ$ disorder.

rotations. It might be a combination of all these. Consider now the diffraction profiles for the $k = 3n$ reflections $130, \bar{2} 01, 200, \bar{1} 31, \bar{2} 02, 131, \bar{1} 32,$ and 201 (see the high-angle region of Fig. 10.10) that lie between 34° and 39° 2θ (Fig. 10.21 B, C, and D). If the pattern for this diffraction region looks like Fig. 10.21B, then the structure is disordered by turbostratic defects. If it resembles Fig. 10.21C, randomly distributed $n120^\circ$ rotations along Z are responsible for the disorder evident in the pattern of Fig. 10.21A. Alternatively, the $k = 3n$ diffraction profile may be best matched by Fig. 10.21D, in which case rotational disorder of the $n60^\circ$ kind dominates. You will have to “read between the lines” if a real experimental pattern shows diffraction effects

intermediate among these more-or-less end member examples. To do better

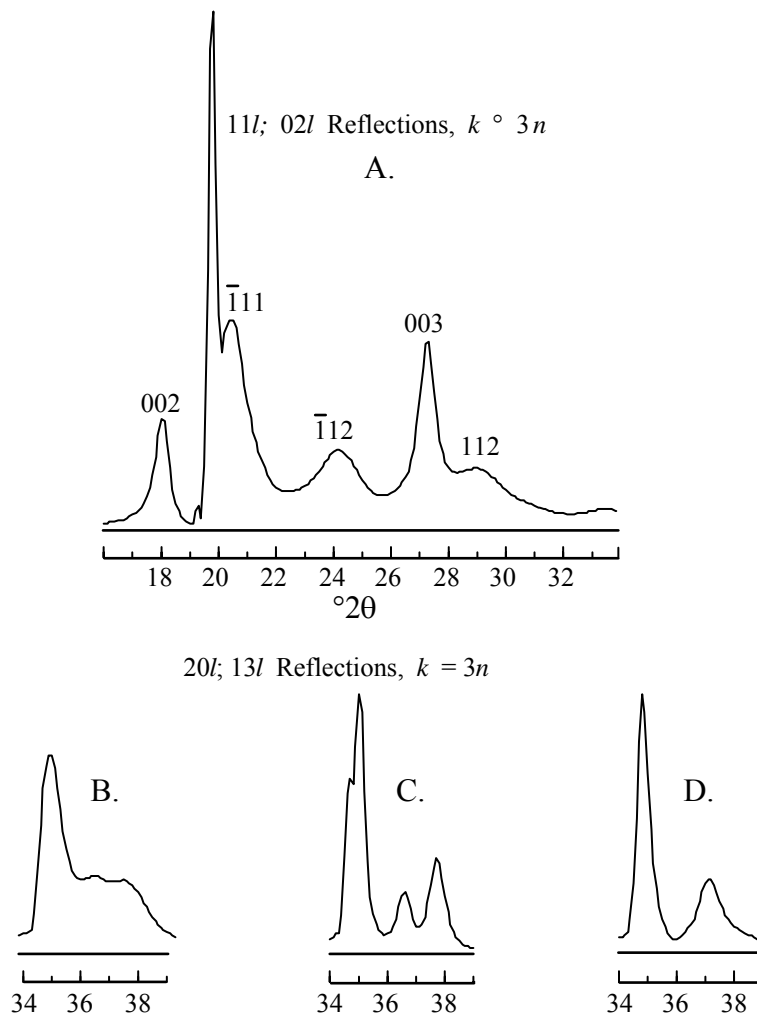


Figure 10.21. An example of the interpretation of a three-dimensional powder XRD pattern for a disordered *tv IM* illite.

than that, the only recourse is to model the diffraction pattern by computer calculations, and adjust the disorder parameters until a good fit is obtained between the calculated and experimental results.

CONCLUSIONS

1. Turbostratic defects that occur across smectite interlayer positions in I/S diffuse all the three-dimensional reflections. In the limit where scattering is restricted to single 2:1 layers, the three-dimensional scattering pattern is marked by asymmetrical bands whose heads roughly correspond to 2θ angles of “prism” reflections like the 110,

020, 130, 200, 040, 220, etc.

2. Rotational disorder is caused by randomly distributed layer rotations of $n120^\circ$ or, more rarely, $n60^\circ$. The $n120^\circ$ rotations broaden and weaken $k \neq 3n$ reflections like the $11l$ and $02l$ sequences, but have only slight effects on the $k = 3n$ peaks such as the $20l$ and $13l$ series. It is this type of disorder that produces illites for which the term *IMd* should be restricted.
3. Disorder of the $n60^\circ$ kind (n is an odd number) can be identified by a tendency of the peaks at $\approx 36.6^\circ$ and $\approx 37.7^\circ$ 2θ to merge into a single peak at about 37° 2θ .
4. Rotational disorder produces a continuous series that separates the pure *IM* polytype from the totally disordered species that has been called *IMd*. Modern nomenclature is inadequate to deal with this series, and in most of the literature, structures are identified as *IM* even though they contain significant amounts of disorder.
5. The well-known *trans*-vacant illite or mica unit cell is common in illite, but so is the newly identified *cis*-vacant variety. These illite types can occur as physical mixtures or as components of interstratifications. They are distinguished by the positions and intensities of the $11l$ and $02l$ reflections.
6. Many or even most specimens of I/S will display all the types of disorder discussed in this chapter: mixed-layering, rotational disorder, and *cis/trans* interstratification.
7. These types of disorder can be identified and quantified if the time is taken to prepare proper samples for X-ray analysis and if attention is paid to diffractometer operating parameters—particularly, the use of long count times in the step-scan procedures. To quote the phrase often used by athletes, “we’ll have to step up to the next level,” to sort these structures out and assign geological meaning to them.

REFERENCES

- Bailey, S. W. (1975) Cation ordering and pseudosymmetry in layer structures: *Am. Mineral.* **60**, 175-87.
- Bailey, S. W. (1988) X-ray diffraction identification of the polytypes of mica, serpentine, and chlorite: *Clays and Clay Minerals* **36**, 193-213.
- Brindley, G. W. (1980) Order-disorder in clay mineral structures: in Brindley, G. W., and Brown, G., editors, *Crystal Structures of Clay Minerals and Their X-Ray Identification*, Monograph **5**, Mineralogical Society, London, 125-95.
- Brindley, G. W., and Méring, J. (1951) Diffraction des rayons X par les structures en couches

- desordonnees: *Acta Cryst.* **4**, 441-47.
- Drits, V. A., Plançon, B. A., Sakharov, B. A., Besson, G., Tsipursky, S. I., and Tchoubar, C. (1984) Diffraction effects calculated for structural models of K-saturated montmorillonite containing different types of defects: *Clay Minerals* **19**, 541-61.
- Drits, V. A., and Tchoubar, C. (1990) *X-Ray Diffraction by Disordered Lamellar Structures*: Springer-Verlag, New York, 371 pp.
- Drits, V. A., Weber, F., Salyn, A. L., and Tsipursky, S. I. (1993) X-ray identification of one-layer illite varieties: Application to the study of illites around uranium deposits of Canada: *Clays and Clay Minerals* **41**, 389-98.
- Grathoff, G.H., and Moore, D.M. (1996) Illite polytype quantification using WILDFIRE™ calculated patterns: *Clays and Clay Minerals*, **44** (in press).
- Lee, M., Lewandowski, J., and Kinzel, M. (1995) Reservoir heterogeneity due to fault related diagenesis in N.W. Germany: *Abstracts with Program*, **27** no. 6., Geological Society of America, New Orleans, A-251 (abstract).
- Méring, J. (1975) Smectites: in Gieseking, J.E., editor, *Soil Components, Vol 2. Inorganic Components*: Springer-Verlag, New York, 97-119.
- Méring, J., and Oberlin, A. (1967) Electron-optical study of smectites: *Clays and Clay Minerals*, 17th Nat. Conf., Pergamon Press, 3-25.
- McCarty, D. K., and Reynolds, R. C., Jr. (1995) Rotationally disordered illite/smectite in Paleozoic K-bentonites: *Clays and Clay Minerals* **43**, 271-84.
- Nadeau, P. H., Wilson, M. J., McHardy, W. J., and Tait, J. M. (1984) Interstratified clays as fundamental particles: *Science* **225**, 923-25.
- Reynolds, R. C. (1992) X-ray diffraction studies of illite/smectite from rocks, and <1μm oriented powder aggregates: The absence of laboratory-induced artifacts: *Clays and Clay Minerals* **40**, 387-396.
- Reynolds, R. C. (1993) Three-dimensional powder X-ray diffraction from disordered illite: Simulation and interpretation of the diffraction patterns: in Reynolds, R.C., and Walker, J.R., editors, *Computer Applications to X-Ray Diffraction Methods*: Clay Minerals Society Workshop Lectures, Vol. **5**, 44-78.
- Reynolds, R. C. (1994) WILDFIRE©, *A Computer Program for the Calculation of Three-Dimensional Powder X-Ray Diffraction Patterns for Mica Polytypes and their Disordered Variations*: R. C. Reynolds, 8 Brook Rd., Hanover, NH.
- Reynolds, R. C., and Thomson, C. H. (1993) Illite from the Potsdam Sandstone of New York: A probable noncentrosymmetric mica structure: *Clays and Clay Minerals* **41**, 66-72
- Sakharov, B. A., Besson, G., Drits, V. A., Kamenava, M. Yu, Salyn, A. L. and Smoliar, B. B. (1990) X-ray study of the nature of stacking faults in the structure of glauconites: *Clay Minerals* **25**, 419-35.
- Smith, J. V., and Yoder, H. S. (1956) Experimental and theoretical studies of the mica polymorphs: *Mineral. Mag.* **31**, 209-35.
- Tsipursky, S. I., and Drits, V. A. (1984) The distribution of octahedral cations in the 2:1 layers of dioctahedral smectites studied by oblique-texture electron diffraction: *Clay Minerals* **19**, 177-93.
- Zvyagin, B. B., Robotnof, V. T., Sidorenko, O. V., and Kotelnikov, D. D. (1985) Unique mica with noncentrosymmetric layers: *Izvestiya Akad. Nauk SSSR, Geol.* **35**, 121-24 (in Russian).